DISCLAIMER

This report was prepared as an account of work sponsored by an agency of the United States Government. Neither the United States Government nor any agency thereof, nor any of their employees, makes any warranty, express or implied, or assumes any legal liability or responsibility for the accuracy, completeness, or usefulness of any information, apparatus, product, or process disclosed, or represents that its use would not infringe privately owned rights. Reference herein to any specific commercial product, process, or service by trade name, trademark, manufacturer, or otherwise does not necessarily constitute or imply its endorsement, recommendation, or favoring by the United States Government or any agency thereof. The views and opinions of authors expressed herein do not necessarily state or reflect those of the United States Government or any agency thereof. Reference herein to any social initiative (including but not limited to Diversity, Equity, and Inclusion (DEI); Community Benefits Plans (CBP); Justice 40; etc.) is made by the Author independent of any current requirement by the United States Government and does not constitute or imply endorsement, recommendation, or support by the United States Government or any agency thereof.

Radiological Releases from Novel Fuel Forms in Advanced Reactors During Severe Accidents for Consequence Analyses

Prepared for
US Department of Energy

M. D. Shah

Oak Ridge National Laboratory

February 2026
ORNL/SPR-2026/4449

OAK RIDGE NATIONAL LABORATORY
MANAGED BY UT-BATTELLE FOR THE US DEPARTMENT OF ENERGY

ORNL/SPR-2026/4449

Nuclear Nonproliferation Division

RADIOLOGICAL RELEASES FROM NOVEL FUEL FORMS IN ADVANCED REACTORS DURING SEVERE ACCIDENTS FOR CONSEQUENCE ANALYSES

M. D. Shah

February 2026

Prepared by
OAK RIDGE NATIONAL LABORATORY
Oak Ridge, TN 37831
managed by
UT-BATTELLE LLC
for the
US DEPARTMENT OF ENERGY
under contract DE-AC05-00OR22725

CONTENTS

LIST OF FIGURES

LIST OF TABLES

ABBREVIATIONS

ATWS	anticipated transient without scram
DLOFC	depressurized loss of forced circulation
DRACS	direct reactor auxiliary cooling system
FHR	fluoride salt–cooled high-temperature reactor
FLiBe	$2LiF–BeF_2$
HPR	heat pipe–cooled reactor
HTGR	high-temperature gas-cooled reactor
LOCA	loss-of-coolant accident
LOHS	loss of heat sink
MSR	molten salt–cooled reactor
PyC	pyrolytic carbon
RCCS	reactor cavity cooling system
SBO	station blackout
SFR	sodium-cooled fast reactor
SNL	Sandia National Laboratories
TOP	transient overpower
TRISO	tristructural isotropic
ULOF	unprotected loss of flow
UTOP	unprotected transient overpower

ACKNOWLEDGMENTS

The author would like to thank the Advanced Reactor Safeguards and Security Program within the US Department of Energy's Office of Nuclear Energy for sponsoring this work. The author would also like to thank the subject matter experts at Oak Ridge National Laboratory and Sandia National Laboratories for their valuable review of this report.

1. INTRODUCTION

Various advanced reactor developers are exploring the potential for reductions in the size of physical security forces and emergency planning zones. These reductions are based on robust fuel forms and inherently safe reactor designs. However, such reductions in physical protection measures could increase the risk of sabotage. To assess the possibility of reducing these measures, sabotage-induced radiological consequence analyses were carried out. These analyses considered accident scenarios that were beyond design basis accidents and overly conservative (Shah, 2025a; Shah, 2025b; Shah and Hartanto, 2026), yielding very large release fractions. These fractions, which can be used to evaluate physical protection and emergency planning requirements, have been crudely determined and applied as demonstrations for a sodium-cooled fast reactor (SFR) (Shah and Hartanto, 2025a), a high-temperature gas-cooled reactor (HTGR) (Shah and Hartanto, 2025b), a heat pipe–cooled reactor (HPR) (Shah and Hartanto, 2025c), and a molten salt–cooled reactor (MSR) (Shah et al., 2026).

A Sandia National Laboratories (SNL) team used MELCOR[1]—a fully integrated severe accident analysis code—to demonstrate the code's capability to analyze advanced (i.e., not light water–cooled) reactors (including a fluoride salt–cooled high-temperature reactor [FHR]) and calculate radiological releases to the environment during severe accidents (Wagner et al., 2022a, 2022b, 2022c, 2023a, and 2023b). Although the analyses were carried out to demonstrate MELCOR's growing capability, the release source terms were estimated for advanced reactors, providing valuable insights into the accident progression and radiological releases. These findings from prior SNL studies, including estimated source terms and related sensitivity studies, were leveraged to derive source terms for postulated sabotage-induced accidents. Insights from these sensitivity studies informed the scaling of SNL's estimated source terms for the defined accident scenarios. The derived release fractions for the severe accident scenarios for the respective reactor designs can be used to perform more nuanced dose consequence analyses to evaluate the reactors' physical protection and emergency planning zone requirements. These analyses are in accordance with the risk-informed, performance-based approach proposed under 10 CFR Part 53.

This study builds on the prior source term analyses and associated sensitivity studies by SNL to derive time-dependent and design-informed release fractions. Section 2 describes the diverse advanced reactor designs analyzed by the SNL team. Section 3 discusses the severe accident analyses, the release fractions calculated, and the limitations and assumptions of the demonstration project. Section 4 presents the release percentages derived for the hypothetical sabotage-induced severe accidents at the advanced reactors. Section 5 summarizes the study's findings and conclusions.

[1] https://www.sandia.gov/MELCOR/

2. ADVANCED REACTOR DESIGNS

Table 1 lists key reactor design details for the five advanced reactors analyzed by the SNL team as part of the US Nuclear Regulatory Commission's source term demonstration project. The reactor designs vary with respect to fuel form, enrichment, cladding, moderator, coolant, operating pressure, and coolant inlet/outlet temperature, among other characteristics.

Table 1. Design details for the five advanced reactors

	FHR (Wagner et al., 2022a)	HTGR (Wagner et al., 2022b)	HPR (Wagner et al., 2022c)	SFR (Wagner et al., 2023a)	MSR (Wagner et al., 2023b)
Reactor type	Fluoride salt–cooled high-temperature reactor	High-temperature gas-cooled reactor	Heat pipe–cooled reactor	Sodium-cooled fast reactor	Molten salt–cooled reactor
Reactor design	University of California, Berkeley Mark 1	Pebble Bed Modular Reactor	INL Design A, adapted from LANL MegaPower	Advanced Burner Test Reactor	Molten Salt Reactor Experiment
Thermal power (MW)	236	400	5	250	10
Fuel form	TRISO with UCO kernels, but used UO_2 data	TRISO UO_2 kernels	UO_2	U-TRU (20%)	UF_4-based fuel salt
Enrichment	19.9%	9.6%	19.75%	16.5%, 20.7% (TRU)	34.5%
Cladding	Silicon carbide	Silicon carbide	Stainless steel	HT-9	—
Moderator	Graphite	Graphite	—	—	Graphite
Coolant	FLiBe	Helium	Potassium	Sodium	LiF-BeF_2-ZrF_2-UF_2
Operating/ vessel pressure (MPa)	Near atmospheric	9	Near atmospheric (0.1)	Near atmospheric (0.135)	Near atmospheric
Coolant inlet/outlet temperature (°C)	600–700	500–900	650–750	355–510	635–668

Note: INL = Idaho National Laboratory; LANL = Los Alamos National Laboratory; TRISO = tristructural isotropic; TRU = transuranic; and FLiBe = 2LiF–BeF_2.

3. ACCIDENT ANALYSES: DEMONSTRATION

This section outlines key factors that influence the start of radiological releases and release magnitudes, covering fuel melting and boiling temperatures, safety systems, and release pathways. Additionally, the section discusses insights from the source term analyses, including the severe accident analyzed, release fractions calculated, and limitations and assumptions.

3.1 TEMPERATURE THRESHOLDS

Table II lists key temperatures, relevant to severe accidents, that determine the start and magnitude of radiological releases in advanced reactors. For example, although the melting point of SiC (2,830°C)[2] is higher than that of UO_2 kernels (2,800°C), the SiC layer in tristructural isotropic (TRISO) fuel fails much sooner because of the shrinkage of the buffer layer (Demkowicz et al., 2018) (Figure 1). Subsequently, the inner pyrolytic carbon (PyC) layer fractures, resulting in a concentrated chemical attack (primarily by palladium) on the SiC layer and the consequent failure of the outer PyC layer.

Table II. Key temperatures that determine the start and magnitude of radiological releases

	FHR (Wagner et al., 2022a)	HTGR (Wagner et al., 2022b)	HPR (Wagner et al., 2022c)	SFR (Wagner et al., 2023a)	MSR (Wagner et al., 2023b)
Key temperatures (°C)	FLiBe boils at ~1,310; UO_2 kernels melt at 2,800; graphite sublimates at 3,600	UO_2 kernels melt at 2,800; graphite sublimates at 3,600	Boiling limit for potassium heat pipe is around 1,050; cladding and heat pipes fail when fuel temperature reaches 1,377	Sodium saturation temperature is 872 (local saturation at 941); fuel melts at 1,350; steel cladding fails at 1,414	FLiBe boils at ~1,340; negligible Cs vaporization occurs with fuel salt temperature <975

Note: FLiBe = $2LiF–BeF_2$.

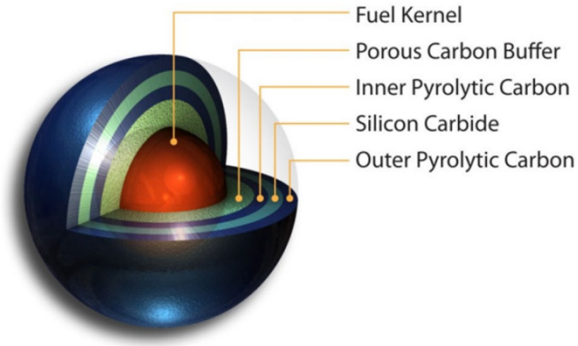

Figure 1. TRISO coating layers. Reproduced from Wagner et al. (2022b) with permission from SNL.

Figure 2 illustrates the TRISO fuel failure fraction curve derived based on the UO_2 TRISO fuel in the German Arbeitsgemeinschaft Versuchsreaktor (AVR) (reproduced from Wagner et al., 2022b). Note that UCO TRISO fuel is expected to have superior performance compared to UO_2 TRISO fuel because UCO kernels form less of the CO that influences the failure of the SiC layer in TRISO pebbles (Wagner et al., 2022a). Similarly, in an SFR, the sodium coolant saturates from 872°C (average) to 941°C (local; higher

[2] https://www.chemicalbook.com/article/silicon-carbide-general-properties-preparation-grades.htm

than average because it is dependent on local pressure). If the fuel temperature exceeds this temperature, heat transfer improves during boiling but leads to instability in coolant flow and local dryout and ultimately exacerbates accident progression. After fuel starts to melt at about 1,350°C, radionuclides are released from the fuel pin to the primary system through a leak in the fuel pin cladding pressure boundary around 1,400°C before the cladding fails at around 1,413°C.

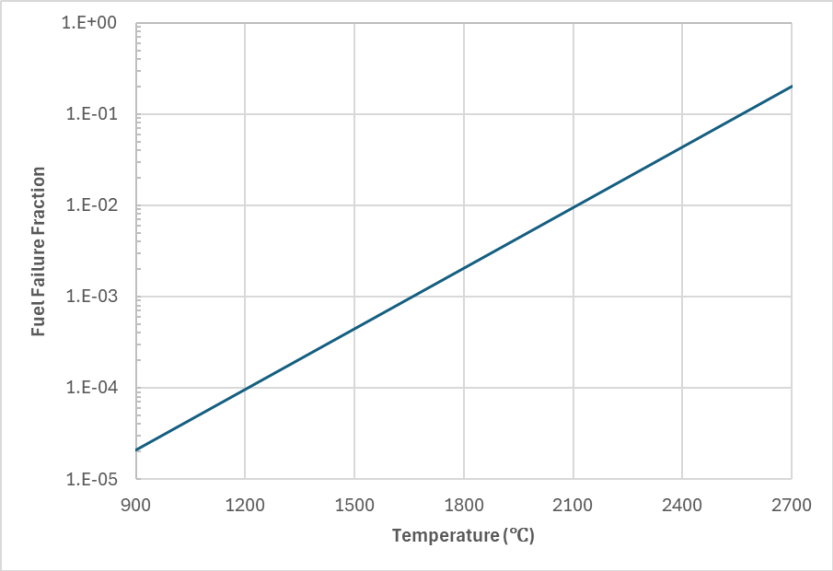

Figure 2. TRISO fuel failure fraction curve as a function of temperature. Reproduced from Wagner et al. (2022b) with permission from SNL.

3.2 RELEASE BARRIERS AND RELEASE MECHANISM

Table III details the release barriers for each of the advanced reactors. These barriers include the primary release barriers of coating layers for TRISO fuel and of cladding for metal/oxide fuel. For the molten salt–fueled reactors, the primary release barrier for nongaseous radionuclides is the molten salt. Depending on the reactor design, the release barrier can include coolant, such as molten salt (FHR) or metal coolant (FHR); the reactor vessel; the guard vessel (SFR) and/or reactor vessel/cavity; the gas retention and vapor condensing tank (MSR); and the containment or reactor building. Generally, the coolant (molten salt or sodium), reactor vessel and/or retention and condensing tanks, and reactor structures provide surface areas on which released radionuclides can settle and be deposited, enabling them to retain radionuclides within the plant.

Alternatively, radionuclide releases begin with the failure of TRISO coatings (TRISO-based reactors) and cladding (SFR and HPR) and/or the volatilization of salt (FHR and MSR) within the primary system or reactor building. Releases to the environment would be through direct (containment or reactor building bypass) and leakage pathways, driven by accident progression. For example, depressurization in the HTGR and HPR and the volatilization of salt can drive out radionuclides, and potential salt and water interactions in the FHR and MSR can generate steam and pressurize the cavity and reactor building, driving out radionuclides. However, the driving force in advanced reactors is not anticipated to be as severe as in light-water reactors, in which the large inventory of water can generate substantial steam (Lebel et al., 2022; Morreale et al., 2023; Shah et al., 2022), among other factors. Moreover, depending on the design, the reactor vessel or cavity may be located below grade, which could limit leakage to the environment.

Table III. Release barriers in advanced reactors

	FHR (Wagner et al., 2022a)	HTGR (Wagner et al., 2022b)	HPR (Wagner et al., 2022c)	SFR (Wagner et al., 2023a)	MSR (Wagner et al., 2023b)
Release barriers	Coating layers; molten salt; reactor vessel; reactor cavity; shield dome	Coating layers; reactor pressure vessel; reactor cavity; confinement building	Cladding or coating layers; reactor vessel; reactor building	Cladding; coolant; reactor vessel; guard vessel; containment cavity; containment dome	Molten salt; reactor vessel; drain/overflow tank; gas retention and vapor condensing tank; reactor cell; reactor building

3.3 REACTOR PROTECTION SYSTEMS

Table IV lists the major active and passive reactor safety systems and contributors to negative reactivity feedback. For the severe accident analyses, the primary and secondary heat removal systems were not credited; however, these systems could possibly mitigate, to a certain extent, even beyond design basis accidents. Safety systems that could operate passively, such as the direct reactor auxiliary cooling system (DRACS) and reactor cavity cooling system (RCCS), were also considered. Similarly, manual operator initiation or actuation following a certain delay was considered. For example, reactor shutdown can be achieved manually by inserting control rods. Although there are few contributors to reactivity feedback, the two most significant are fuel-related (temperature and density) coefficients and the thermal behavior of the sodium coolant (SFR), moderator, and/or reflector. These passive reactivity feedback mechanisms can help prevent reactor runaway during a spurious positive reactivity insertion accident. A passive, natural circulation–driven cooling system can complement these mechanisms and help limit accident progression. However, if the control rods are not inserted within a certain time, the reactor can return to power after a period of time, offsetting the negative reactivity feedback.

Table IV. Reactor protection systems in advanced reactors

	FHR (Wagner et al., 2022a)	HTGR (Wagner et al., 2022b)	HPR (Wagner et al., 2022c)	SFR (Wagner et al., 2023a)	MSR (Wagner et al., 2023b)
Reactor safety systems	Control rods; primary and secondary heat removal system; DRACS; refractory reactor cavity liner system	Control rods; primary and secondary heat removal system; RCCS	Control rods; primary and secondary heat removal system	Control assemblies; primary and secondary heat removal systems; DRACS; guard vessel cooling system	Control rods; primary and secondary heat exchangers; gas retention tank; vapor condensing tank
Negative reactivity feedback contributors	Fuel, moderator, molten salt, xenon	Fuel, moderator, xenon	Fuel, reflector, xenon	Fuel, sodium	Fuel, moderator, xenon

3.4 REACTOR ACCIDENTS AND SOURCE TERMS

Table V details the reactor accidents and relevant details from the source demonstration project. For the FHR (Wagner et al., 2022a), anticipated transient without scram (ATWS), station blackout (SBO), and loss-of-coolant accident (LOCA) scenarios were analyzed. The ATWS scenario involved a loss of on-site power and failure to insert the control rods. The peak fuel temperature was 996°C at 27.7 h (less than the 2LiF–BeF_2 [FliBe] boiling limit of about 1,310°C) without a DRACS, and no releases were estimated.

The SBO scenario involved a loss of on-site power with the control rods inserted. Without passive heat removal through a DRACS, the fuel temperature continued to rise, and the peak temperature was 1,089°C at 48 h. The estimated TRISO fuel failure fraction (based on the UO_2 data) increased to 4.9×10^{-5} over 48 h from the manufacturing defect fraction of 1×10^{-5}. This increase resulted in a cesium release fraction of 9×10^{-5} at 48 h, all of which was assumed to be retained within the molten salt. The LOCA scenario involved a leak in a 7.62 cm (3 in.) diameter pipe; the salt level in the reactor vessel decreased at a rate based on the LOCA break size. For a 100% break size LOCA, the fuel temperature reached the FLiBe saturation temperature at 24 h and was greater than 2,800°C at 54 h. Without considering the vaporization of radionuclides retained within the molten salt, the iodine release fraction to the environment was less than 2×10^{-4} at 54 h, and the cesium release fraction was less than 1×10^{-4}. For a 10% LOCA accounting for cesium vaporization (pool chemistry model), the cesium vaporized fraction was less than 2×10^{-4} at 24 h, and the release fraction to the environment was about 4×10^{-7} at 24 h (vs 4×10^{-12} for a 75% LOCA without accounting for vaporization).

For the HTGR (Wagner et al., 2022b), postulated depressurized loss of forced circulation (DLOFC) and ATWS scenarios were analyzed. The DLOFC scenario included a break in the hot leg exiting the reactor vessel with the active heat removal system unavailable and control rods inserted for scram. The maximum fuel temperature was 1,634°C at 35 h, which resulted in an overall TRISO failure fraction of 1.6×10^{-4} at 37 h. Most of the releases from fuel were retained within the vessel and the reactor building. The release fractions to the environment for iodine and cesium were 9×10^{-10} and 2×10^{-5} at 72 h, respectively. A 50% degraded thermal conductivity of graphite was estimated to increase iodine and cesium releases to the environment by roughly an order of magnitude at 168 h. The unavailability of an RCCS had a minor influence on the release fractions. Similarly, with a 100× higher building leakage rate and an external wind speed of 10 m/s, the iodine and cesium releases were estimated to increase by an order of magnitude. In the ATWS scenario, strong negative reactivity feedback from Doppler and fuel density was accompanied by moderator and xenon feedback as the accident progressed. The peak fuel temperature was 1,203°C at 1 h, resulting in only a minor increase in the TRISO failure fraction (~4×10^{-5}) over the simulated daylong accident.

For the HPR (Wagner et al., 2022c), transient overpower (TOP) and loss of heat sink (LOHS) scenarios were assessed. The TOP scenario considered a spurious positive reactivity insertion without the insertion of control/shutdown rods. The fuel temperature gradually increased to the boiling limit of the potassium heat pipes (1,050°C), which degraded heat transfer and caused local heatup of fuel (peak temperature of 1,925°C); this resulted in cladding failure (at 1,377°C) and, afterward, manual insertion of control rods after the high radiation signal was triggered (about 1 h into the accident). Subsequently, the temperature decreased to about 925°C by 24 h. The iodine release fraction to the environment was estimated at 8×10^{-6} at 24 h. With a 100× higher building leakage rate and an external wind speed of 10 mph, the iodine release fraction was estimated to increase to 1×10^{-3}, an increase of about 125×. For the LOHS scenario, two variations were simulated: one with the insertion of control rods and another without (ATWS). The maximum fuel temperature in both variations was significantly less than the cladding melting temperature over the first 24 h because of strong negative reactivity feedback from Doppler and fuel elongation accompanied by reflector expansion after the initial temperature increase. Overall, no source term was estimated based on the LOHS scenario.

For the SFR (Wagner et al., 2023a), unprotected TOP (UTOP), unprotected loss of flow (ULOF), and blocked fuel assembly accident scenarios were investigated. The UTOP scenario simulated the introduction of positive reactivity with failure to insert control assemblies but with active heat removal available. The heat removal capability, in conjunction with strong negative reactivity feedback from Doppler, fuel density, and sodium void and density, mitigated the accident and provided a sufficient margin (144°C) relative to the local sodium saturation temperature (941°C). The ULOF scenario simulated the loss of active heat removal with failure to insert control assemblies to terminate the fission reaction. Similar to the UTOP scenario, this scenario resulted in no source term for the simulated 27.7 h of the accident; the peak fuel temperature (802°C) was still less than the sodium saturation temperature, even when no passive DRACS was available. The blocked fuel assembly scenario considered the inlet sodium coolant flow being blocked and the reactor tripping shortly thereafter. The coolant in the channel boiled off (starting at 897°C) within a few seconds and raised the fuel temperature to more than the steel cladding melting point (1,414°C). Fuel releases via leakage from the vessel through the cover gas line into the containment and then to the environment were estimated to be very small for xenon (i.e., a release fraction of 5×10^{-7} at about 2 h).

For the MSR (Wagner et al., 2023b), a fuel salt spill from the reactor vessel into the reactor building through a break in the pipe was analyzed; several variations were included, such as a coincident water spill. The maximum fuel temperature was less than 635°C within the first 10 min after the spill, and the fuel gradually cooled down; thus, negligible vaporization (e.g., $<1 \times 10^{-8}$ for cesium) was estimated. However, 100% of nobles gases and 10% of other radionuclides (e.g., iodine, cesium) were assumed to be released into the reactor cell atmosphere over the first 100 s of the spill. After this release from the fuel salt, about 0.2% of noble gases (NGs), 0.02% of iodine and cesium iodide, 0.003% of cesium fluoride, and less than 1×10^{-8} of cerium and other aerosols were estimated to escape out to the environment in 24 h. When reactor cell auxiliary filter ventilation was accounted for, the amount of NGs released to the environment increased to 25%. Similarly, releases of other radionuclides increased by an order of magnitude (e.g., CsF at 0.09%, Ce at 1×10^{-9}). For a coincident water spill with gas retention and vapor condensing tanks available, radionuclide releases to the environment decreased because fission products were retained within the retention and condensing tanks. For example, release percentages for NGs were estimated at 0.08% at 27.7 h compared to 0.2% at 24 h with no water spill. With a 100× higher building leakage rate and external wind, the releases of radionuclides, especially the NGs, increased significantly.

Table V. Reactor accidents and relevant details from the source demonstration project

	FHR (Wagner et al., 2022a)	HTGR (Wagner et al., 2022b)	HPR (Wagner et al., 2022c)	SFR (Wagner et al., 2023a)	MSR (Wagner et al., 2023b)
Accident types analyzed	ATWS; SBO; LOCA (5% to 100% of a 7.62 cm [3 in.] diameter pipe)	DLOFC; ATWS	TOP; LOHS	UTOP; ULOF; blocked fuel assembly	Fuel salt spill with and without a coincident water spill
[a] Releases from the fuel	ATWS: very small release, but retained within the molten salt SBO: small release, but retained within the molten salt Cs: 9×10^{-5} at 48 h LOCA (75%): I: 7×10^{-2} at 54 h; Cs: 5×10^{-2} at 54 h	DLOFC: I: 1.6×10^{-8} at 24 h; 1.6×10^{-8} at 168 h Cs: 8×10^{-5} at 24 h; 9×10^{-4} at 168 h Ag: 99% released With degraded thermal conductivity: I: 7×10^{-8} at 24 h; 1.6×10^{-7} at 168 h Cs: 4×10^{-4} at 24 h; 4×10^{-3} at 168 h	TOP: 1.4% of the iodine inventory	UTOP: none ULOF: none Blocked assembly: 97% of NGs; <6% of Cs/I (assumed 25% of NGs in gas plenums and 5% of Cs/I in the sodium bond) from an assembly, which represents 1.85% of the total inventory	Salt spill (assumed): NGs: 100% Others: 10%
Leakage area/ pathways	Shield dome; turbine-side Total: 56.12 cm^2 (8.7 $in.^2$)	Reactor building; passive flapper (pressure relief valve—prevents overpressurization damage to the building during blowdown) Total: 20.6 cm^2 (3.3 $in.^2$)	Vessel to reactor building: 10.3 cm^2 Reactor building to environment: 11.6 cm^2	Containment to environment: 0.1% vol/day at 69 kPa(g) (10 psig)	Reactor cell: 0.1 cm^2 (1.83 mm diameter); reactor building Total: 12.32 cm^2 (two 1.4 cm diameter)
Release fractions/ percentages (to environment)	LOCA (75%): I: 2×10^{-4} at 54 h Cs: 8×10^{-5} at 54 h 10% LOCA with pool chemistry model: Cs: 4×10^{-7} at 24 h	DLOFC (with degraded thermal conductivity): I: 1×10^{-8} at 168 h Cs: 1.7×10^{-4} at 168 h	TOP: I: 8×10^{-6} at 24 h With 100× building leakage and external wind of 10 mph: 1×10^{-3} at 24 h	NGs: 5×10^{-7} at 2 h; Others: none (nonconservative estimate; assumes retention of volatile products in the sodium)	Salt spill (no coincident water) at 24 h: NGs: 0.2% I_2: 0.02% CsI: 0.02% CsF: 0.003% Others: $<1 \times 10^{-8}$

[a] When using TRISO-based fuel, there is a failure fraction of 1×10^{-5} due to manufacturing defects, which may contribute to small releases during normal operations. When using UO_2 with cladding, there are no releases during normal operations.

4. POSTULATED SABOTAGE-INDUCED SEVERE ACCIDENTS

Building on SNL's source term analyses and associated sensitivity studies, a postulated scenario was identified for each advanced reactor design. These scenarios represent sabotage-induced accidents, combining physical and cyber attacks. For example, the LOCA with DRACS unavailable could be a result of cyber attack on the primary system followed by physical attack that renders the DRACS nonoperational. In these scenarios, active heat removal systems were not credited, and passive heat removal systems were either not available or their capacity was considered degraded. Moreover, the scenarios assumed a large containment leakage rate and sustained external wind at the site, which increases infiltration and exfiltration, driving larger releases to the environment compared to releases considering the design basis containment leakage rate. Table VI provides detail on the postulated sabotage-induced accidents and the derived release fractions obtained by scaling SNL's calculated released fractions while accounting for findings from the sensitivity studies and some assumptions.

Table VI. Postulated sabotage-induced accidents and derived release fractions

	FHR (Wagner et al., 2022a)	**HTGR (Wagner et al., 2022b)**	**HPR (Wagner et al., 2022c)**	**SFR (Wagner et al., 2023a)**	**MSR (Wagner et al., 2023b)**
Scenario for consequence analysis	LOCA with DRACS unavailable, pool chemistry model considered, large containment building leakage, and external wind	DLOFC with degraded graphite thermal conductivity, large containment building leakage, and limited RCCS	TOP with manual control rod insertion by an operator after the high radiation signal is triggered, large containment building leakage, and external wind	Blocked assemblies with radionuclide vaporization from sodium, large containment building leakage, and external wind	Fuel salt spill with radionuclide vaporization from molten salt, building ventilation and auxiliary filters available, large containment building leakage, and external wind
Time-dependent releases for the scenario (cumulative release fractions)	**0 to 12 h:** no release **12 to 24 h:** I, NG: 4×10^{-6} Cs, others: 4×10^{-7} **24 to 36 h:** I, NG: 8.34×10^{-5} Cs, others: 8.34×10^{-6} **36 to 48 h:** I, NG: 1.69×10^{-3} Cs, others: 1.69×10^{-4}	**0 to 12 h:** I, NG: 6×10^{-10} Cs, Ag, others: 1×10^{-7} **12 to 24 h:** I, NG: 6×10^{-9} Cs, Ag, others: 6×10^{-6} **24 to 36 h:** I, NG: 1.6×10^{-8} Cs, Ag, others: 6×10^{-5} **36 h to 48 h:** I, NG: 2.6×10^{-8} Cs, Ag, others: 1.7×10^{-4}	**UO_2** **0 to 12 h:** I, NG: 1.7×10^{-4} Others: 1.7×10^{-5} **12 to 24 h:** I, NG: 3×10^{-4} Others: 3×10^{-5} **24 to 36 h:** I, NG: 3.3×10^{-4} Others: 3.3×10^{-5} **36 to 48 h:** I, NG: 3.5×10^{-4} Others: 3.5×10^{-5} **TRISO fuel** On the conservative side, same as the releases for the HTGR	**0 to 12 h:** NG: 5.9×10^{-4} I: 2.9×10^{-5} Others: 5.9×10^{-6} **12 to 24 h:** NG: 1.1×10^{-3} I: 5.4×10^{-5} Others: 1.1×10^{-5} **24 to 36 h:** NG: 1.7×10^{-3} I: 8.4×10^{-5} Others: 1.7×10^{-5} **36 to 48 h:** NG: 4.7×10^{-3} I: 2.4×10^{-4} Others: 4.7×10^{-5}	**0 to 12 h:** NG: 0.15 I: 4×10^{-4} Cs: 3×10^{-4} Others: 1×10^{-5} **12 to 24 h:** NG: 0.22 I: 5×10^{-4} Cs: 4×10^{-4} Others: 1×10^{-5} **24 to 36 h:** NG: 0.27 I: 6×10^{-4} Cs: 4.5×10^{-4} Others: 1×10^{-5} **36 to 48 h:** NG: 0.3 I: 7×10^{-4} Cs: 5×10^{-4} Others: 1×10^{-5}

For the FHR, a LOCA scenario with the passive DRACS unavailable and volatilization of radionuclides from molten salt accounted for (pool chemistry model) was considered. This postulated accident should increase fuel temperature from 750°C to more than FLiBe saturation within the first 24 h and to more than 2,000°C by 48 h. This simulated accident might result in TRISO fuel failure fractions of 2×10^{-4} at 24 h and 2×10^{-2} at 48 h, resulting in iodine and cesium releases of 4% and 2%, respectively, from the fuel. With vaporization from molten salt, the assumed larger containment building leakage rate, and external wind, the release fraction to the environment for iodine and NGs is expected to be 1.69×10^{-3} at 48 h; for cesium and others it is expected to be 1.69×10^{-4}.

For the HTGR, a DLOFC with degraded graphite thermal conductivity, the assumed larger containment building leakage rate, and a limited RCCS was considered. The TRISO fuel failure fraction is anticipated to reach 3×10^{-4} by 24 h and 7×10^{-4} by 48 h, resulting in release fractions from the fuel of 7×10^{-8} and 8×10^{-8} at 24 and 48 h for iodine, respectively, and 4×10^{-4} and 1.7×10^{-3} at 24 and 48 h for cesium, respectively. The environmental release fraction for iodine and NGs is expected to be 2.6×10^{-8} by 48 h; the release fraction for cesium, silver, and other radionuclides is expected to be 1.7×10^{-4}. Given the HTGR's lower power density (4.8 MW/m^3 compared to 22.7 MW/m^3 for the FHR) and the higher thermal inertia of its reflectors compared to the FHR, the HTGR peak fuel temperature was lower, resulting in limited releases of radionuclides with lower diffusivities compared to the FHR.

For the HPR, a TOP scenario with manual control rod insertion after the high radiation signal is triggered was considered. The reactor building was assumed to have a larger containment building leakage rate and to be located at a site with sustained external wind. The iodine release fraction to the environment is expected to be 3×10^{-4} at 24 h and 3.5×10^{-4} at 48 h for UO_2 fuel in cladding. For the HPR with TRISO-based fuel, the release fractions identified for the HTGR provide a conservative estimate.

For the SFR, a postulated accident involving several blocked fuel assemblies, radionuclide vaporization from sodium, the assumed larger containment building leakage rate, and external wind was considered. The assemblies in this case accounted for about 10% of all assemblies. The release estimates from fuel and the release fractions to the environment were scaled to account for a higher number of blocked assemblies (from 1.85% to 10% of all assemblies) and higher leakage rates. The release fractions to the environment at 48 h were expected to be 4.7×10^{-3} for NGs and 2.4×10^{-4} and 4.7×10^{-5} for iodine and other radionuclides, respectively.

For the MSR, a postulated accident involving molten fuel salt spilling into the reactor cell, auxiliary filters and reactor building ventilation running, the assumed larger containment building leakage rate, and external wind was considered. The releases were primarily driven by the radionuclides transferred to the reactor cell atmosphere during the spill and the vaporization of radionuclides from the molten fuel salt. The release fractions to the environment at 48 h is expected to be 30% for NGs, 0.07% for iodine, 0.05% cesium, and 0.001% for other radionuclides.

Overall, these postulated accidents are low-probability, high-consequence events, and the derived release fractions are time-dependent and design-informed, supporting more nuanced consequence analyses for evaluating physical protection and emergency planning zone requirements.

5. SUMMARY

Using the MELCOR analyses carried out by the SNL team under the US Nuclear Regulatory Commission's advanced reactor source term demonstration project, this study determined potential sabotage-induced severe accidents that could be consequential. These scenarios represent low-probability, high-consequence events, possibly incorporating a combination of both physical and cyber attacks. In these accidents, active heat removal systems were not available, and passive systems were either unavailable, or their capability was assumed to be degraded. Moreover, a containment building leakage rate larger than the design basis containment leakage rate and the presence of on-site external wind were considered; these are factors that can drive large releases to the environment. The release fractions for dose-significant radionuclides were determined based on SNL's source term analyses and associated sensitivity studies. The derived release fractions are design-informed and time-dependent and can be used in performing more nuanced radiological consequence analyses to evaluate physical protection and emergency planning zone requirements for advanced reactors.

REFERENCES

Demkowicz, P. A. et al. 2018. "Key Results from Irradiation and Post-Irradiation Examination of AGR-1 UCO TRISO Fuel." *Nuclear Engineering and Design* (329): 102–109. https://doi.org/10.1016/j.nucengdes.2017.09.005.

Lebel, L. et al. 2022. "Development of CANDU-Specific Operational Intervention Levels." *Annals of Nuclear Energy* 168: 108890. https://doi.org/10.1016/j.anucene.2021.108890.

Morreale, A. C. et al. 2023. "Sensitivity Analysis of Severe Accident Calculations for the Estimation of CANDU-Specific OILs." *Annals of Nuclear Energy* 182: 109592. https://doi.org/10.1016/j.anucene.2022.109592.

Shah, M. D. et al. 2022. "Assessment of Filtered Containment Venting Strategies for Mitigating Severe Accident Consequences at a Generic Single-Unit CANDU." *Journal of Nuclear Engineering and Radiation Science* 9 (1): 011701. https://doi.org/10.1115/1.4055258.

Shah, M. D. 2025a. "Assessment of Fission Product Release Behavior in Sodium-Cooled Fast Reactors for Consequence Assessment." *Transactions of the American Nuclear Society* 132 (1): 824–27. https://www.ans.org/pubs/transactions/article-58667/.

Shah, M. D. 2025b. "Assessment of Fission Product Release in High-Temperature Gas-Cooled Reactors Using TRISO Fuel for Radiological Consequence Assessment." Advances in Nuclear Nonproliferation Technology and Policy Conference (ANTPC 2025), Washington, DC, November 9–12, 2025.

Shah, M. D., and D. Hartanto. 2025a. "Consequence Analyses of Sabotage-Induced Radiological Releases in Sodium-Cooled Fast Microreactors." *Nuclear Engineering and Design* 444, 114360. https://doi-org.ornl.idm.oclc.org/10.1016/j.nucengdes.2025.114360.

Shah, M. D., and D. Hartanto. 2025b. "Consequence Analyses of Sabotage-Induced Radiological Releases in High-Temperature Helium-Cooled Prismatic Microreactors." *Progress in Nuclear Energy* 191, 106083. https://doi-org.ornl.idm.oclc.org/10.1016/j.pnucene.2025.106083.

Shah, M. D., and D. Hartanto. 2025c. "What might radiological consequences from sabotage-induced releases look like in heat pipe-cooled microreactors?" *Nuclear Engineering and Technology* (forthcoming).

Shah, M.D. et al. 2026. *Comparative Assessment of Radiological Consequences from Sabotage-Induced Releases in Diverse Microreactor Designs*. ORNL/SPR-2025/4326. Oak Ridge National Laboratory.

Shah, M. D., and D. Hartanto. 2026. "Assessment of Fission Product Release Behavior in Liquid-Fueled Molten Salt Reactors for Radiological Consequence Assessment." ANS Annual Conference, Denver, Colorado, May 31-June 3, 2026.

Wagner, K. et al. 2022a. *MELCOR Accident Progression and Source Term Demonstration Calculations for a FHR*. SAND2022-2751. Sandia National Laboratories. https://www.nrc.gov/docs/ML2214/ML22144A197.pdf.

Wagner, K. et al. 2022b. *MELCOR Accident Progression and Source Term Demonstration Calculations for HTGR*. SAND2022-2750. Rev. 1. Sandia National Laboratories. https://www.nrc.gov/docs/ML2214/ML22144A190.pdf.

Wagner, K. et al. 2022c. *MELCOR Accident Progression and Source Term Demonstration Calculations for a Heat Pipe Reactor*. SAND2022-2745. Sandia National Laboratories. https://www.nrc.gov/docs/ML2214/ML22144A188.pdf.

Wagner, K. et al. 2023a. *MELCOR Accident Progression and Source Term Demonstration Calculations for a Sodium Fast Reactor (SFR)*. SAND2023-10830. Sandia National Laboratories. https://www.nrc.gov/docs/ML2328/ML23285A093.pdf.

Wagner, K. et al. 2023b. *MELCOR Accident Progression and Source Term Demonstration Calculations for a Molten Salt Reactor*. SAND2023-01803. Sandia National Laboratories. https://www.nrc.gov/docs/ML2311/ML23117A094.pdf.